JACS
JOURNAL OF THE AMERICAN CHEMICAL SOCIETY

ARTICLE

pubs.acs.org/JACS

Lamellar Assembly of Cadmium Selenide Nanoclusters into Quantum Belts

Yi-Hsin Liu,[†] Fudong Wang,[†] Yuanyuan Wang,[†] Patrick C. Gibbons,[‡] and William E. Buhro*[,†]

[†]Department of Chemistry, [‡]Department of Physics, and the Center for Materials Innovation, Washington University, St. Louis, Missouri 63130-4899, United States

Supporting Information

ABSTRACT: Here, we elucidate a double-lamellar-template pathway for the formation of CdSe quantum belts. The lamellar templates form initially by dissolution of the CdX_2 precursors in the *n*-octylamine solvent. Exposure of the precursor templates to selenourea at room temperature ultimately affords $(CdSe)_{13}$ nanoclusters entrained within the double-lamellar templates. Upon heating, the nanoclusters are transformed to CdSe quantum belts having widths, lengths, and thicknesses that are predetermined by the dimensions within the templates. This template synthesis is responsible for the excellent optical properties exhibited by the quantum belts. We propose that the templated-growth pathway is responsible for the formation of the various flat, colloidal nanocrystals recently discovered, including nanoribbons, nanoplatelets, nanosheets, and nanodisks.

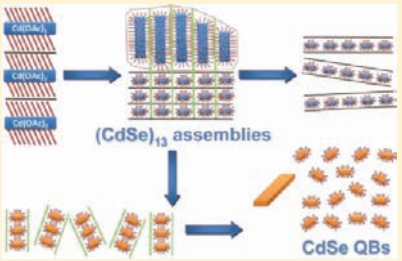

INTRODUCTION

Herein, we report the detailed pathway for the formation of CdSe quantum belts (QBs). We show that CdX_2 (X = OAc, I) compounds in long-chain primary-amine solvents form lamellar structures that serve as templates for the formation of $(CdSe)_{13}$ nanoclusters. The resulting amine-template nanocluster composites spontaneously organize into double-lamellar assemblies. Recrystallization of the nanoclusters within the templates affords CdSe quantum belts (QBs) having widths and thicknesses determined by the periodicities of the double-lamellar nanostructures. This template synthesis affords excellent control over QB thickness and accounts for the excellent optical properties of the QBs.

The preparation of CdSe nanoribbons, nanoplatelets, and nanosheets was reported independently by Hyeon and co-workers[1,2] and by Ithurria and Dubertret[3,4] under synthetic conditions similar to those employed here. We subsequently demonstrated that CdSe quantum belts, which were morphologically comparable to the nanoribbons of Hyeon and co-workers,[1] exhibit photoluminescence quantum yields of 30 ± 10%.[5] Such high photoluminescence efficiencies are unprecedented for pseudo-one-dimensional colloidal semiconductor nanostructures and indicate that excitons are effectively transported over micrometer-scale diffusion distances parallel to the QB long axes.

A remarkable aspect of the nanoribbon, nanoplatelet, nanosheet, and QB syntheses is the flat, layer-like, morphologies of the nanocrystals. Normally, nanocrystals grown in solution have dot[6] or rod-like morphologies,[7−10] or wire morphologies if appropriate catalyst nanoparticles are present,[11−13] or a self-assembly mechanism is active.[14−17] Additionally, the reaction temperatures employed (∼70−120 °C) are quite low for nanocrystal syntheses. Consequently, the mechanisms or pathway by which these nanostructures form must be unusual.

Considerable insight into this pathway was provided by Hyeon and co-workers, who demonstrated that dissolution of $CdCl_2$ in primary-amine solvents resulted in the formation of lamellar $CdCl_2(amine)_2$ complexes.[2] They showed that such lamellar precursors served as templates for the formation of planar CdSe nanosheets. In a subsequent paper, Hyeon and co-workers determined that $(CdSe)_{33,34}$ and $(CdSe)_{13}$ nanoclusters were intermediates in the process.[18]

Here, we elucidate a similar pathway for the formation of CdSe QBs with experimental detail that accounts for the morphology produced. We demonstrate that the templates adopt double-lamellar structures that are responsible for the QB morphologies. We confirm that the intermediate nanoclusters are indeed entrained within the template structures. We show that the conversion of $(CdSe)_{13}$ nanoclusters to CdSe QBs is reversible. We also show that the double-lamellar assemblies of $(CdSe)_{13}$ nanoclusters and CdSe QBs dissociate or unbundle in different dimensions, the $(CdSe)_{13}$ nanoclusters into lateral sheets and the QBs into vertical stacks. Finally, we report the synthesis of QBs of two specific thicknesses and demonstrate that the thinner QBs are intermediates in the formation of the thicker QBs.

EXPERIMENTAL SECTION

Materials. *n*-Octylamine (*n*-OA) from Aldrich (+99%) and Alfa Aesar (99%), selenourea (99.9%, metal basis) from Alpha Aesar, $Cd(OAc)_2 \cdot 2H_2O$ (Aldrich), trioctylphosphine (TOP) from Sigma-Aldrich (97%), and oleylamine (or *cis*-9-octadecenylamine) from TCI (>40.0% by GC) and Sigma-Aldrich (technical grade, 70%) were used as received and stored under N_2. Toluene from Sigma-Aldrich

Received: July 20, 2011
Published: September 09, 2011

dx.doi.org/10.1021/ja206776g | *J. Am. Chem. Soc.* 2011, 133, 17005–17013

(CHROMASOLV, for HPLC, ≥99.9%) was purged with dry N_2 for at least 1 h and stored under N_2 prior to use.

Synthesis of CdSe Nanocluster Assemblies (NCAs). All synthetic procedures were conducted under dry N_2. In a typical reaction, cadmium acetate dihydrate [$Cd(OAc)_2 \cdot 2H_2O$] (80 mg, 0.30 mmol) was dissolved in *n*-octylamine (*n*-OA, 6.7 g, 0.052 mol) in a septum-capped tube and heated in a 68 °C oil bath for 1 h. In a glovebox, selenourea (67 mg, 0.54 mmol) was dissolved in *n*-OA (2.8 g, 0.022 mol) in a septum-capped amber vial. The vial was removed from the glovebox and placed in a benchtop sonicator bath for 10−20 min to achieve dissolution of the selenourea.

The selenourea solution was injected into the $Cd(OAc)_2$ solution to provide Se/Cd ratios in the ranges of 1.73−1.82 at room temperature (20−25 °C). During the first hour, the reaction mixture underwent multiple color changes from colorless (0 min) to orange-yellow (viscous, 0−15 min), yellow (cloudy, 15−120 min) to greenish-yellow (cloudy, > 120 min) with some brown precipitate. After 2 h, the solution became nearly clear and colorless upon formation of a greenish-yellow precipitate. Slow stirring of the sealed tube under ambient conditions for another 12−44 h resulted in a completely white precipitate. At this stage, the supernatant was pink, and the white precipitate contained "as-made" CdSe nanoclusters, composed of $(CdSe)_{13}$ with some $(CdSe)_{19}$ and $(CdSe)_{33,34}$.

Annealing of as-made CdSe nanoclusters proceeded in a 64−85 °C oil bath for 1 h. After annealing, the reaction solution turned dark red, and a small amount of black or gray precipitate had mixed in with the white precipitate, which remained in the bottom one-third of the reaction volume. The black solid and red solution color were due to elemental Se, which was subsequently converted to TOP═Se by addition of TOP. (In our experience, selenourea is unstable with respect to elemental Se in the presence of light or air, and its decomposition is accelerated in the presence of a primary amine.) After TOP (2−3 mL) was injected, the red supernatant quickly turned clear and colorless, and the remaining precipitate was white. This white precipitate after the annealing process was referred to as "annealed" CdSe nanoclusters.

Both as-made and annealed CdSe nanoclusters were further purified by washing with a TOP solution (5−10% w/w in toluene) prior to characterization. The white precipitates were centrifuged in a benchtop centrifuge (700*g*) for 1−3 min, and the supernatant was discarded. The purification process was repeated 1−2 times by adding TOP−toluene solution or toluene. This white precipitate was referred to as "purified" CdSe nanoclusters. Anal. Calcd for $C_8H_{19}CdNSe$: C, 29.97; H, 5.97; N, 4.37. Found: C, 30.89; H, 5.84; N, 4.57. All values are given as percentages.

The purified nanoclusters were dispersed in the TOP−toluene solution or toluene for further characterization.

Unbundling of CdSe NCAs. The unbundling process was conducted in oleylamine−toluene solution. For analysis of the "unbundled" CdSe NCAs, an aliquot (ca. 0.1 mL) from the dispersion of annealed, purified CdSe NCAs was diluted into oleylamine−toluene (20%, w/w, 1 mL). The unbundling process required 5−7 days at room temperature or was expedited by sonication for 5−20 min. Unbundled CdSe NCAs afforded a clear colorless or pale yellow (from oleylamine) dispersion. The NCAs were flocculated from this dispersion by 1−2 drops of acetone (<0.1 mL) in air, and the resulting mixture was centrifuged in a benchtop centrifuge (700*g*) for ≥15 min to produce a white unbundled NCA precipitate. The supernatant was discarded. An additional portion of toluene (1 mL) and acetone (0.05 mL) was added to the precipitate, and the mixture was centrifuged as above. The supernatant was again discarded, and the white NCA precipitate was redispersed into toluene (2 mL) to afford a clear, colorless dispersion of unbundled NCAs for TEM analysis.

Direct Synthesis of Thinner CdSe QBs. All synthetic procedures were conducted under dry N_2. Thinner CdSe QBs were synthesized by a modification of the procedure of Peng and co-workers.[19] A Schlenk flask was loaded with $Cd(OAc)_2 \cdot 2H_2O$ (72 mg, 0.27 mmol) and *n*-OA (6.3 g, 48 mmol) and transferred to a 65−68 °C oil bath for 1 h with stirring. In a glovebox, a solution of selenourea (58 mg, 0.47 mmol) in *n*-OA (1.35 g, 10.4 mmol) was prepared in a septum-capped vial. Vigorous sonication (10−15 min) was required to dissolve all of the selenourea, which was accompanied by a color change from colorless to pink or reddish-brown. This solution was immediately injected into the Schlenk flask held at 65 °C. In various trials, the reaction stoichiometry was adjusted to provide Se/Cd ratios in the range of 1.68−1.74.

The reaction proceeded with color changes from colorless (0 min) to yellow, orange (viscous), and then to greenish-yellow (3−4 h). Stirring was continued (18−24 h) at 63−68 °C, followed by stirring at an elevated temperature (90−110 °C) for 1 h. The resulting CdSe QBs formed a greenish-yellow dispersion mixed with a black precipitate, characterized as elemental selenium by XRD. The elemental Se was removed by injecting TOP (0.5 mL) in N_2-purged toluene (10 mL) into the flask. The dispersion of bundled QBs was then stored at room temperature under N_2 for subsequent analyses.

Direct Synthesis of Thicker CdSe QBs. All synthetic procedures for thicker QBs were conducted under the same general conditions for thinner QB synthesis, except for the reaction temperature, which was elevated to 118−122 °C (as compared to 63−68 °C for the thinner QBs). The formation of thicker QBs proceeded with more rapid color changes from colorless (0 min) to yellow, orange (viscous, 3 min), yellow (12 min), and then back to orange (>91 min). Stirring was continued for another 18−24 h. Annealing was conducted at an elevated temperature (138−140 °C) for 1 h. The resulting CdSe QBs formed an orange dispersion mixed with a black precipitate, characterized as elemental selenium by XRD. The elemental Se was removed by injecting TOP (0.5 mL) in N_2-purged toluene (10 mL) into the flask. The dispersion of bundled QBs was stored at room temperature under N_2 for subsequent analyses.

Unbundling of CdSe QBs by *n*-Oleylamine. This unbundling procedure resulted in purification, ligand exchange, and unbundling of CdSe QBs. An aliquot (0.2 g) of the annealed CdSe QB dispersion prepared by the synthetic procedure above was transferred to a septum-capped vial. A solution of oleylamine (1.5 mL, 10% w/w in toluene) was added, and the vial was shaken vigorously a few times and allowed to stand on the benchtop for a few hours. During this period, most of the QBs settled to the bottom third of the vial as a cloudy suspension. The upper two-thirds was clear and greenish-yellow for thinner QBs or orange for thicker QBs, indicating that this fraction contained some unbundled QB dispersion. The upper, clear fraction (ca. 1 mL) was removed by pipet and set aside or discarded.

The purification procedure was continued by adding another portion of the oleylamine solution (ca. 1 mL) to the remaining QB suspension in the vial. After purification, the unbundling process was conducted in two different ways, which led to similar results. The unbundling process was expedited to 5−11 min under a mild sonication, or, as before, the vial was shaken vigorously a few times and allowed to stand on the benchtop overnight. During this period, the dispersion of bundled QBs settled into the bottom two-thirds of the vial. The upper, clear, yellow fraction (ca. 0.5 mL) was removed for subsequent TEM analysis. The resulting precipitate of "partially unbundled" QBs was used for spectroscopic analyses on the same day to retain a high PL quantum yield. Dilution of the precipitate with oleylamine solution by 10−20× (to ca. 10−20 mL) afforded a clear dispersion of unbundled QBs.

RESULTS

Formation of Lamellar CdX_2(*n*-octylamine)$_x$ Assemblies. As noted above, Hyeon and co-workers previously reported the synthesis of lamellar $CdCl_2(amine)_2$ complexes under preparative

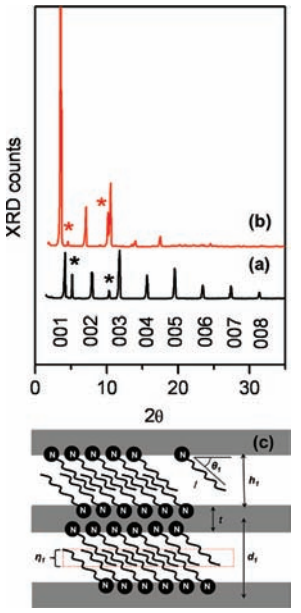

Figure 1. XRD patterns of (a) CdI_2(*n*-octylamine)$_x$ and (b) $Cd(OAc)_2$-(*n*-octylamine)$_x$ complexes. Lamellar structures of different spacings proposed in (c) correspond to minor (asterisked) and major diffraction patterns in (a) and (b).

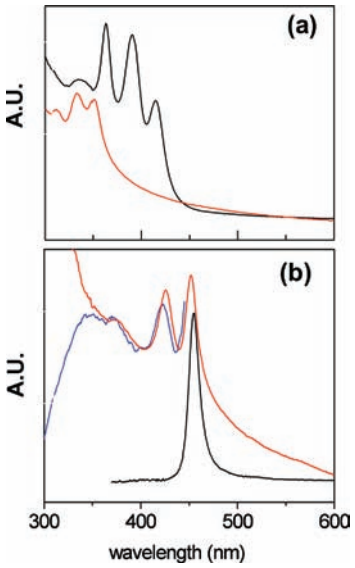

Figure 2. Spectral evolution upon transformation from CdSe nanoclusters to thinner CdSe quantum belts (QBs). (a) UV−visible extinction spectra of CdSe nanoclusters after 2 h (black curve) and 20 h (red curve) at room temperature. The absorptions for $(CdSe)_{13}$ (336, 352 nm), $(CdSe)_{19}$ (363 nm), and $(CdSe)_{33,34}$ (389 nm) are assigned according to the literature.[33] The feature at 413 nm may correspond to $(CdSe)_{66}$.[33] (b) Photoluminescence (black curve), extinction (red curve), and photoluminescence excitation (blue curve) spectra of transformed CdSe QBs.

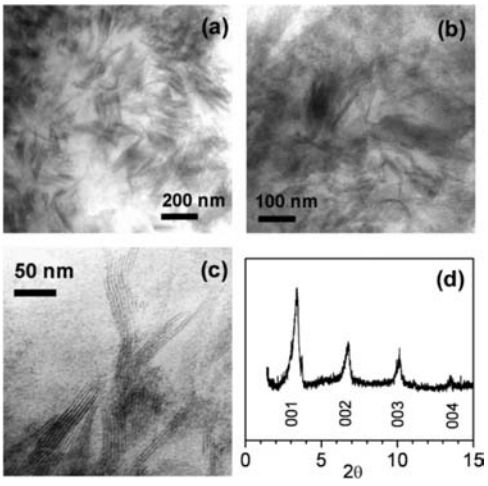

Figure 3. Representative TEM images (a−c) and a low-angle XRD pattern (d) of bundled $(CdSe)_{13}$ nanocluster assemblies (NCAs).

conditions similar to those employed here.[2] Lamellar structures were confirmed by SAXS data and proposed to adopt configurations like that in Figure 1c, in which planar $CdCl_2$ layers are spaced apart by monolayers of coordinated amines. Hyeon and co-workers demonstrated that the interlayer spacing *d* was dependent on the alkyl chain length of the primary-amine ligands in the expected manner.

We prepared a corresponding CdI_2(*n*-octylamine)$_x$ complex in *n*-octylamine solvent at 70 °C. Subsequent cooling of the reaction mixture precipitated CdI_2(*n*-octylamine)$_x$ as a white solid, which was analyzed by low-angle XRD (Figure 1a). A series of first- and higher-order reflections was observed, corresponding to an interlayer spacing *d* of 2.25 ± 0.06 nm. Two additional reflections were present that could be assigned to a *d* spacing of 1.72 nm, presumably corresponding to a minor structural component of the CdI_2(*n*-octylamine)$_x$ sample. As demonstrated in Figure 1c, the *d* spacing depends on the tilt angle θ and the interpenetration fraction η, leading to a kind of structural isomerism or alternate phase formation. The existence of such phase admixtures has been previously observed in lamellar structures.[20]

A $Cd(OAc)_2$(*n*-octylamine)$_x$ complex was similarly prepared in *n*-octylamine at 70 °C. The low-angle XRD pattern of this precursor material exhibited first- through fifth-order reflections corresponding to a *d* spacing of 2.61 ± 0.07 nm. As above, other minor reflections were presumably due to minor isomeric phases.[20] The lamellar morphology of the $Cd(OAc)_2$(*n*-octylamine)$_x$ complex, and particularly its interlamellar van der Waals galleries, made it a good host structure and Cd precursor for CdSe nanoclusters and, ultimately, for CdSe QBs, as detailed below.

Generation of Intratemplate $(CdSe)_{13}$ Nanoclusters. The $Cd(OAc)_2$(*n*-octylamine)$_x$ precursor and selenourea were allowed to react in *n*-octylamine at 20−25 °C. Color changes from colorless through orange-yellow, green-yellow, and yellow were observed during the first hour, suggesting the formation of CdSe nanoclusters of various sizes. A UV−visible spectrum recorded after 2 h contained characteristic features for $(CdSe)_{13}$, $(CdSe)_{19}$, and $(CdSe)_{33,34}$ nanoclusters (Figure 2a). Over the same time scale, the solution was observed to gel, and then to deposit a light-yellow precipitate containing the nanoclusters.

Stirring of the mixture was continued, and aliquots of the stirred suspension were removed and diluted in a TOP−toluene solution (see Experimental Section) for UV−visible spectroscopy. A spectrum obtained after 20 h showed the effective disappearance of the absorbances for $(CdSe)_{19}$ and $(CdSe)_{33,34}$, with prominent absorbances for $(CdSe)_{13}$ remaining (Figure 2a). The conversion of the initially formed, larger nanoclusters to the smaller $(CdSe)_{13}$

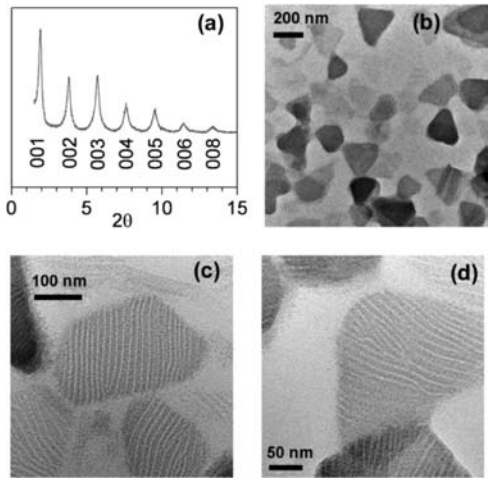

Figure 4. Unbundling of $(CdSe)_{13}$ NCAs. (a) An XRD pattern of partially unbundled $(CdSe)_{13}$ NCAs. (b–d) Representative TEM images of almost completely unbundled $(CdSe)_{13}$ NCAs showing single- and multiple-sheet structures.

parallels the previous observation of Hyeon and co-workers.[18] At this stage, the precipitate containing the $(CdSe)_{13}$ nanoclusters was white.

The reaction mixture containing the $(CdSe)_{13}$ nanoclusters was heated at 64–85 °C (1 h, and then the nanocluster–template assemblies were purified as described in the Experimental Section). Such thermal annealing stabilized the nanoclusters with respect to conversion to QBs (see below) and gave more highly ordered lamellar assemblies (that is, generated the laterally striped domain structure described below). Specimens suitable for XRD and TEM analyses were obtained. TEM images revealed aggregates that appeared to be bundled nanostructures (Figure 3a,b). Features containing parallel fringe patterns were found near the edges of these bundles, consistent with lamellar assemblies (Figure 3c). The low-angle XRD pattern of this material also provided evidence for a lamellar structure, having a *d* spacing of 2.64 ± 0.07 nm (Figure 3d).

The white precipitate containing the $(CdSe)_{13}$ lamellar assemblies was sonicated in a solution of *n*-oleylamine in toluene at 25 °C for 5 min. The precipitate-to-volume ratio was sufficiently high that the precipitate remained largely nondispersed. An XRD pattern of the sonicated precipitate (Figure 4a) revealed that the *d* spacing in the lamellar assemblies had increased from 2.64 to 3.79 ± 0.05 nm as a result of exchange of *n*-octylamine spacers by longer-chain *n*-oleylamine spacers. Similar surfactant-exchange and layer-expansion processes were previously demonstrated by Hyeon and co-workers.[2]

Sonication of the $(CdSe)_{13}$ lamellar assemblies in *n*-oleylamine solutions under more dilute conditions and for longer periods (~10 min) resulted in the dispersion and unbundling of the assemblies. TEM images of the dispersed material contained sheet-like features having pseudotriangular and pseudotrapezoidal shapes (Figure 4b). The contrast of these features varied, suggesting that they corresponded variously to single and multiple layers from the lamellar assemblies. Consequently, the sonication and surfactant exchange caused the unbundling of the lamellar assemblies, releasing single and multilayers into solvent dispersion.

The progress of the unbundling process was monitored by UV–visible spectroscopy. A dispersion was formed by allowing

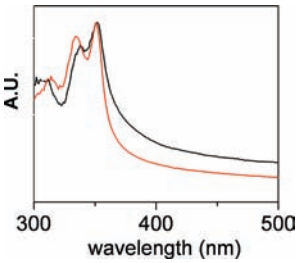

Figure 5. UV–visible extinction spectra of NCAs before and after unbundling. The black curve corresponds to $(CdSe)_{13}$ NCAs after dispersion in oleylamine–toluene overnight. The substantial tailing to longer wavelengths is indicative of bundled structures. The red curve corresponds to $(CdSe)_{13}$ NCAs after sonication in the same solution for 20 min. The reduced extinction intensity above 350 nm indicated unbundling to smaller structures. Both curves are normalized to the maximum peak intensity for comparison.

the $(CdSe)_{13}$ lamellar assemblies to stand in *n*-oleylamine solution overnight without sonication. The spectrum of this dispersion contained the characteristic absorbances of $(CdSe)_{13}$ (330 and 350 nm) and a long tail to longer wavelengths due to scattering (Figure 5). The dispersion was then sonicated for 20 min. The $(CdSe)_{13}$ absorbances were retained in the spectrum, but the scattering tail was greatly diminished. The results indicated the progressive unbundling of the lamellar assemblies to smaller structures less able to scatter light, and strongly suggested that the $(CdSe)_{13}$ nanoclusters were entrained within individual layers from the assemblies.

Further evidence of $(CdSe)_{13}$–nanocluster entrainment was obtained from TEM images of the unbundled material at higher magnification. Images of the lightest-contrast sheet features (presumably single layers) revealed parallel stripe patterns of alternating light and dark domains, having a periodicity of 10–14 nm (Figure 4c,d). The dark domains were considerably wider than the light domains. We surmised that the higher contrast of the dark domains was due to the localization of the heavier-element-containing $(CdSe)_{13}$ nanoclusters in these regions, although individual nanoclusters could not be imaged under these conditions. The light domains were assigned to amine-surfactant regions. Elemental analysis (see Experimental Section) and IR spectroscopy confirmed that no detectable acetate ligands remained in the $(CdSe)_{13}$ lamellar assemblies. Additionally, the width expansion of the lateral domain structure was monitored during the exchange of *n*-octylamine by oleylamine via sonication. As shown in Figure S1 (Supporting Information), the domain widths increased as the shorter *n*-octylamine spacers were replaced by the longer oleylamine spacers.

Significantly, the widths of the darker $(CdSe)_{13}$ domains corresponded closely to the widths of the CdSe QBs subsequently produced from these materials (7–15 nm; see below). The existence of surfactant-separated stripes within individual layers indicated that the $(CdSe)_{13}$–nanocluster assemblies possessed double-lamellar structures in orthogonal dimensions (Figure 6) and strongly suggested that these double-lamellar assemblies were responsible for the belt-like morphologies ultimately obtained.

Conversion of $(CdSe)_{13}$–Nanocluster Assemblies to CdSe Quantum Belts. The reaction mixture containing the $(CdSe)_{13}$–*n*-octylamine assemblies generated at 20–25 °C (see above) was

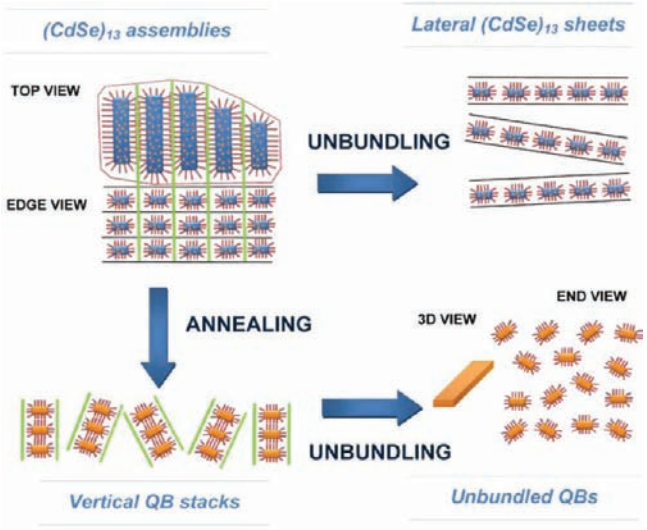

Figure 6. A schematic showing the conversion of the double-lamellar $(CdSe)_{13}$ NCAs to CdSe QBs, and the various unbundling processes that occur. The blue fields represent the host domains within the double-lamellar templates. $(CdSe)_{13}$ nanoclusters are represented as orange dots and CdSe QBs as orange rectangles. The short red lines depict primary-amine surfactant molecules. The black and green lines represent the orthogonal interfaces along which unbundling occurs.

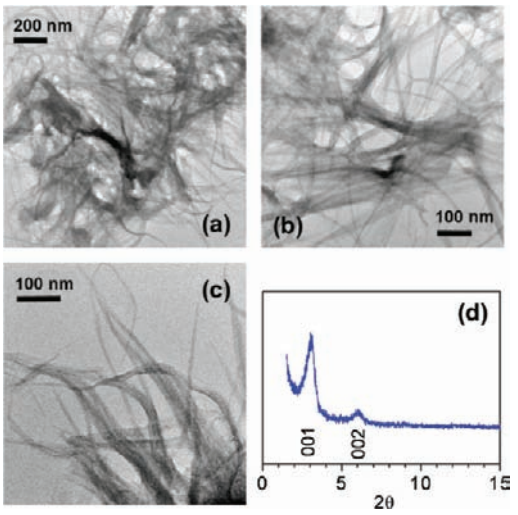

Figure 7. TEM images (a−c) and a low-angle XRD pattern (d) of bundled CdSe QBs obtained by conversion of $(CdSe)_{13}$ NCAs.

heated to 85−98 °C. During this process, the white precipitate turned to green-yellow. Monitoring by UV−visible spectroscopy revealed a conversion of the $(CdSe)_{13}$ nanoclusters that began at 85 °C and became complete at 98 °C. The characteristic absorbances for $(CdSe)_{13}$ were progressively replaced by three new absorbances at 378, 423, and 447 nm (Figure 2b). As previously discussed,[5] these features may be assigned to CdSe QBs or nanosheets, which exhibit nearly identical spectra corresponding to 1D quantum-confinement systems.[5] The CdSe QBs exhibited a single, sharp, band-edge photoluminescence peak (Figure 2b), as previously reported.[5]

TEM images of a QB specimen as prepared above are included in Figure 7a−c. The images contained wispy bundles indicating

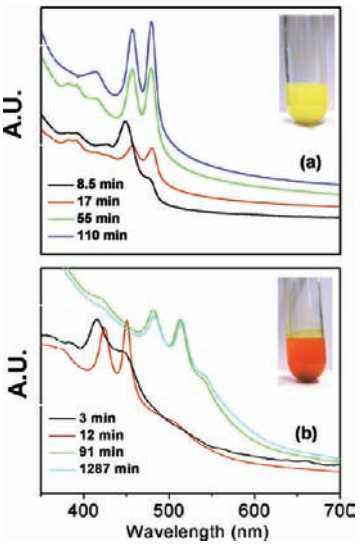

Figure 8. Data corresponding to direct syntheses of CdSe QBs at different temperatures. (a) Extinction spectra recorded during the preparation of thinner CdSe QBs at 64 °C. (b) Extinction spectra recorded during the preparation of thicker CdSe QBs at 118 °C. The inset images are of the respective QB specimens.

that lamellar assemblies remained intact, but with a significantly extended length dimension as compared to those in the images of the $(CdSe)_{13}$ assemblies (see Figure 3). Correspondingly, evidence for lamellar QB assemblies was also obtained by low-angle XRD (Figure 7d), although the lack of a full series of higher-order reflections indicated that these assemblies were less uniformly ordered than those of the precursor or $(CdSe)_{13}$ assemblies. Further characterization of CdSe QBs is given below.

Direct Synthesis of CdSe Quantum Belts. CdSe QBs were also synthesized in a single procedure from the $Cd(OAc)_2$(*n*-octylamine)$_x$ and selenourea precursors in *n*-octylamine at temperatures above 20−25 °C. The process was monitored by UV−visible spectroscopy, and a sequence of nanocluster intermediates culminating in $(CdSe)_{13}$ was observed (Figure 8a), as described above. Interestingly, by this more-direct synthesis, the conversion to QBs was achieved at 45−80 °C, which is below the range of 85−98 °C required for the conversion from preformed $(CdSe)_{13}$. The best synthetic results for these QBs, which we refer to as the thinner QBs, were obtained in the middle of the 45−80 °C range.

When the direct synthesis was conducted near 120 °C, a similar sequence of intermediates was observed (Figure 8b). However, at this higher temperature, the absorbances for the thinner QBs were observed to disappear in time and be replaced by a similar set of absorbances at longer wavelength (425, 485, and 518 nm). This latter conversion was complete within 1.5 h and was accompanied by a color change from yellow to orange. We show below that these spectral features correspond to QBs having distinctly larger thicknesses, which we refer to as the thicker QBs.

The products of the direct syntheses were collected as yellow-green and orange solids for the thinner and thicker QBs, respectively. A low-angle XRD pattern of the thinner QBs evidenced lamellar structures as above (Figure S2). TEM images of the QB−*n*-octylamine assemblies confirmed bundled structures consisting of aligned, face-to-face stacks of QBs (Figure 9).

dx.doi.org/10.1021/ja206776g |*J. Am. Chem. Soc.* 2011, 133, 17005–17013

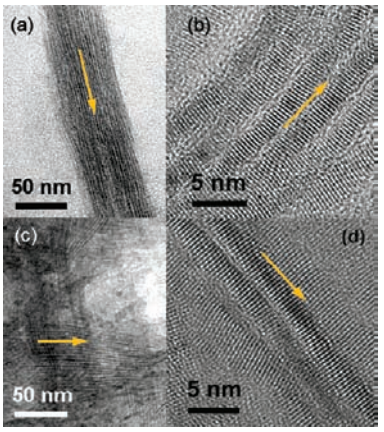

Figure 9. Representative TEM and HRTEM images of bundled CdSe QBs. (a) TEM and (b) HRTEM images of thinner CdSe QBs (1.5−2.0 nm). (c) TEM and (d) HRTEM images of thicker CdSe QBs (2.5−3.0 nm). Yellow arrows in (a−d) indicate length dimension (along [0001] direction) of bundled QBs.

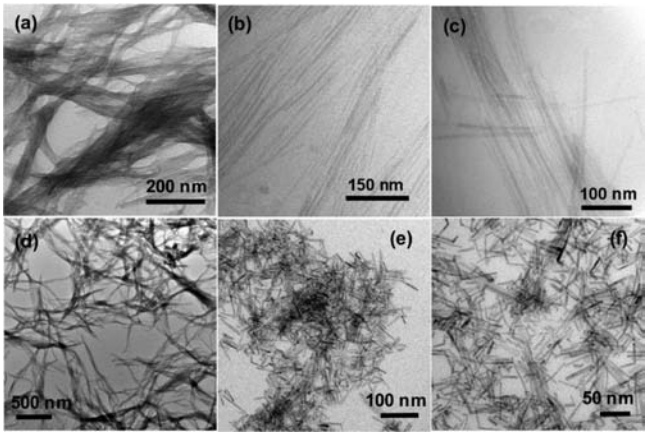

Figure 10. TEM images of bundled and unbundled CdSe QBs. Bundled (a) and unbundled (b,c) thinner CdSe QBs. Bundled (d) and unbundled (e,f) thicker CdSe QBs.

The thicknesses of the QBs were measured from these images and were found to be 1.5−2.0 and 2.5−3.0 nm for the thinner and thicker QBs, respectively. These ranges reflect thickness variations along single QBs and among QBs. Notably, the thickness ranges do not overlap, consistent with the thinner and thicker QBs representing two distinct populations, and with the spectroscopic results discussed above and below (Figures 8b and S2).

The QB−*n*-octylamine assemblies were stabilized by heating at 80 °C, and then unbundled by sonication in *n*-oleylamine according to the procedure used for the $(CdSe)_{13}$ assemblies (see above). The QB assemblies were also unbundled in refluxing *n*-dodecanethiol. However, *n*-dodecanethiol quenched the PL of the QBs, whereas *n*-oleylamine enhanced it, and so the first unbundling procedure was preferred. TEM images before and after unbundling are shown in Figure 10. The broad faces of the QBs were revealed in the unbundled specimens, allowing the widths of the QBs to be measured. They were found to be 5.0−15 nm for both the thinner and the thicker QBs. This range reflects width variations among QBs. Width variations along individual QBs were generally less than 0.5 nm. The lengths of the QBs varied from 0.5 to 1.5 μm.

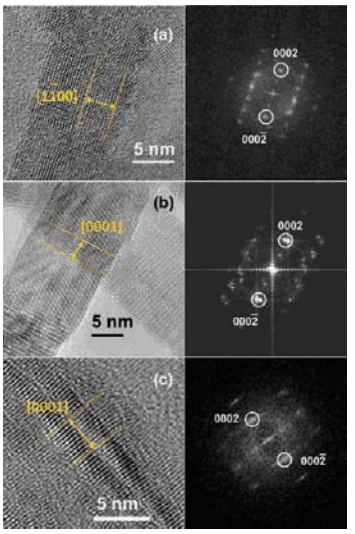

Figure 11. HRTEM images of thicker (a) and thinner (b,c) CdSe QBs (left), and fast Fourier transforms of the images (right). Images a and b are taken normal to the broad top and bottom QB faces, and image c is focused on the thin edges of two stacked QBs. The (11$\bar{2}$0) image plane for (a) and (b) is confirmed by the diffraction patterns in the Fourier transforms, and specifically by the near extinction of the 0001 and 000$\bar{1}$ diffraction spots (the residual intensity results from double diffraction). (The (11$\bar{2}$0) and (2$\bar{1}\bar{1}$0) image planes are members of a crystallographically equivalent set and produce identical diffraction patterns.) The (1$\bar{1}$00) image plane for (c) is also confirmed by the diffraction pattern. The long axis of the QBs therefore lies along [0001], and the width dimension lies along [1$\bar{1}$00]. (a) The yellow lines demarcate 10 lattice fringes along the [1$\bar{1}$00] direction. (b) The yellow lines demarcate 10 lattice fringes along the [0001] direction. (c) The yellow lines demarcate 10 lattice fringes along the [0001] direction.

The high-angle XRD patterns of the thinner and thicker QBs were indexed to the wurtzite crystal structure (Figure S3). Fast Fourier transforms of high-resolution images allowed determination of the crystallographic orientation of the QBs (Figure 11). The long axis of the QBs was found to lie along [0001], the width along [1$\bar{1}$00], and the thickness along [11$\bar{2}$0], as previously reported.[1,2,5]

An experiment was conducted to determine if the thinner CdSe QBs could be converted to the thicker QBs. The direct synthesis of thinner QBs was conducted as described above, and product formation was verified by UV−visible spectroscopy (Figure S4a). The reaction mixture was then heated to 145 °C, and the conversion process was monitored spectroscopically. After approximately 30 min, features for both the thinner and thicker QBs were present in the extinction (absorption) and PL spectra (Figure S4). After approximately 90 min, the features for the thinner QBs had disappeared, and only those for the thicker QBs remained. Observation of this interconversion suggested that the thinner QBs are intermediates in the formation of the thicker QBs.

Another experiment demonstrated a surprising partial reversibility of the templated QB formation. An as-made specimen of bundled, thinner QBs synthesized at 64 °C and exhibiting a normal QB absorption spectrum (like that in Figure 8a) was sonicated at room temperature for 5 min. The absorption spectrum of the sonicated specimen contained prominent features corresponding

to $(CdSe)_{13}$ nanoclusters, the precursor species to QB formation (Figure S5). When an identical as-made QB sample was first annealed in solution at 80 °C (for 1 h), and then subjected to sonication at room temperature for 5 min, the formation of $(CdSe)_{13}$ nanoclusters was not spectroscopically evident (Figure S5). Longer sonication periods were necessary to induce reversal of QB formation for the annealed, stabilized samples. Apparently, QB stability was affected by the uniformity or precise structure of the QB−*n*-octylamine assemblies, and/or the *n*-octylamine−QB ligation, which were influenced by annealing at the higher temperature. Remarkably, the $(CdSe)_{13}$−*n*-octylamine and QB−*n*-octylamine assemblies must be sufficiently close in energy to exhibit an observable thermal equilibrium, and the barrier to their interconversion must also be low.

DISCUSSION

Gaining purposeful morphological control over colloidal nanocrystals is now an area of great interest and activity. Nanocrystal growth from solution typically produces nearly isotropic dot-like morphologies. Rod-shaped nanocrystals are obtained when growth conditions are pushed farther from equilibrium and/or when passivating ligands that stabilize specific crystal facets are employed.[8,21] Nonequilibrium growth has also produced a range of other morphologies, including tetrapods, teardrops, arrows, and other unusual shapes.[9,22] Colloidal nanowires may be grown by catalyzed methods[11−13] or by self-assembly and oriented attachment.[14,19,23]

However, only recently have pseudo-two-dimensional (2D) plate- or sheet-like nanocrystals been obtained. As noted above, these examples include nanoribbons,[16,18] nanoplatelets,[3,4,24,25] nanodisks,[26,27] nanosheets,[2,15,28] and QBs.[5] Interest in such pseudo-2D systems includes the quantum-well-like quantum confinement in only the thickness dimension, and high photoluminescence efficiencies that are indicative of excellent surface structure and passivation.[5] The morphological similarity of the various pseudo-2D nanocrystals, and the large contrast from the more typical pseudo-0D (dots) and pseudo-1D nanocrystals (rods and wires), strongly suggest that they grow by an unconventional mechanism or mechanisms. We propose that the mechanistic pathway depicted in Figure 6 may be generally relevant to the formation of all of these pseudo-2D morphologies, and thus may unify nanoribbon, nanoplatelet, nanodisk, nanosheet, and QB syntheses.

As shown separately by Hyeon and co-workers and the results reported here, CdX_2 precursors in long-chain, primary amine solvents generate lamellar precursor templates.[1] These template structures persist during the subsequent formation of $(CdSe)_n$ nanoclusters, and their ultimate recrystallization to layer-like, pseudo-2D nanocrystals. Although Ithurria and Dubertret do not employ a long-chain, primary amine solvent in their nanoplatelet syntheses, they do use long-chain cadmium myristate precursors, and we suspect that similar lamellar precursor templates may form under their conditions.[4] Indeed, the formation of lamellar reaction templates is a very attractive explanation for the formation of pseudo-2D morphologies.

Weller and co-workers recently reported the formation of thin PbS nanosheets by a 2D oriented-attachment process.[17] They proposed the initial formation of PbS nanocrystals, which subsequently assembled into 2D nanosheets under the direction of densely packed oleic-acid ligand layers on the nanocrystal surfaces, and with the necessary assistance of chlorine-containing cosolvents. The process ultimately afforded lamellar assemblies of PbS nanosheets.

There are clear parallels between the mechanism proposed in Figure 6 and that proposed by Weller and co-workers.[17] Both involve nanocluster/nanocrystal assembly and attachment, and both result in lamellar assemblies. They differ in the proposed sequence of events. Whether these are two distinct mechanisms or variations of the same mechanism is presently unclear.

Recently, Dubertret and co-workers invoked another mechanism for the growth of CdSe nanoplatelets.[4] They proposed a continuous lateral extension of nanoplatelet seeds sustained by Cd and Se precursor reaction. Nanoplatelets found stacked together were uniformly separated by 3.75 nm, which approximates the sum of two oleic-acid chain lengths and one nanoplatelet thickness. The results established that the top and bottom nanoplatelet faces were passivated by oleic-acid monolayers.[4]

There are also parallels between the observations of Dubertret and co-workers and the mechanism outlined in Figure 6. In both cases, the early formation of small nanoclusters/nanoparticles is succeeded by the growth of belt/platelet structures.[4] In both cases, long-chain surfactants are employed, and evidence of mesophase formation is obtained. Determination of whether these are distinct mechanisms or variations of the same mechanism will require further study.

We propose that the stripe-domain width and overall dimensions of the lamellar-template structures (Figure 6) determine the 2D-nanocrystal morphology ultimately produced. Single-lamellar or double-lamellar templates having wide lateral periodicities will produce nanosheets or nanoplatelets. Double-lamellar templates with smaller lateral periodicities will produce nanoribbons or QBs. The lengths of the nanoribbons or QBs will depend on the lateral size of the template structures (specifically, the lateral sheet size in Figure 4).

These template structural aspects cannot yet be rationally controlled, and so specific 2D-nanocrystal morphologies cannot be purposefully synthesized. For example, the lengths of the QBs we report are generally only 0.5−1.5 μm. We hope to extend these lengths so that QBs might perform wire-like functions. Thus, an important future goal is to gain an understanding of the factors that determine the lateral dimensions and spatial periodicities in the templates.

A fascinating aspect of the double-lamellar template structures encountered in this study is the capacity for template unbundling in different geometric dimensions. As shown in Figure 6, disassembly of the $(CdSe)_{13}$−*n*-octylamine assemblies occurs in the lateral dimension, liberating sheets of entrained $(CdSe)_{13}$ nanoclusters. In contrast, conversion of the $(CdSe)_{13}$−*n*-octylamine assemblies to QBs results in disassembly in the vertical dimension, releasing stacks of CdSe QBs (Figure 6). The observation of disassembly in these two dimensions provides strong evidence for the proposed double-lamellar structures.

We propose that the lamellar-template syntheses are responsible for the excellent optical properties exhibited by QBs and nanoplatelets, which have optimized photoluminescence efficiencies of 30−50%.[3−5] We measured a photoluminescence efficiency as high as 42% in one CdSe QB specimen, but the mean value is 30%.[5] Such high values are especially surprising for QBs, as their extended length dimension exposes delocalized excitons[5] to a very large surface area upon which they may encounter trap sites. For comparison, the

highest photoluminescence efficiencies reported for quantum wires having roughly isotropic cross sections are $\leq$0.3%.[5]

In our recent study of QB photoluminescence, surface-defect populations were assessed using a decoration strategy.[5] To our surprise, the surface defects were found to be concentrated on the thin QB edges rather than on the broad top and bottom surfaces, which were largely defect free. Consequently, the excellent QB optical properties are due to the minimization of defective surface area to 14% of the total contained within the edges.

However, the crystallographic differences between the $\{1\bar{1}00\}$ edge and $\{11\bar{2}0\}$ top/bottom facets are quite subtle. Both types are nonpolar surfaces having equal numbers of Cd and Se atoms, with surface Cd−Se dimers arranged in only a slightly different manner.[29] Thus, a crystallographic or surface-structure explanation for the much better passivation of the top and bottom facets in comparison to the edge facets is not apparent. We therefore surmise that the better top and bottom passivation results from the templated-growth pathway.

We propose that lamellar-templated growth enhances QB optical properties in at least two ways. First, the amine templates provide dense passivation to the developing QB facets, which may approach the quality of self-assembled monolayers. Second, the observation of only two, discrete QB thicknesses, and the very narrow QB and nanoplatelet photoluminescence features,[3−5] suggests that the top and bottom facets may be crystallographically flat terraces largely free of steps (ledges) and kinks. These two conditions, dense surface passivation and monolayer flatness, are optimal for minimizing defects and therefore trap sites on the broad top and bottom QB facets.

Finally, we note that the so-called magic-sized $(CdSe)_n$ nanoclusters (as well as their sulfide and telluride congeners) are generally prepared in long-chain, primary-amine solvents.[19,30−32] It is tempting to consider that all of these nanoclusters form within lamellar template structures, and that such templates may be important to their stabilization. We reported here that the nanocluster-to-QB conversion is at least partially reversible. We also reported here that the temperature for conversion from $(CdSe)_n$ nanoclusters to CdSe QBs (64 vs 98 °C) depended on the thermal history of the template system. These observations suggest that the nanoclusters are indeed stabilized within the templates, and that nanocluster stability is strongly influenced by the precise template structure and nanocluster ligation within the template.

CONCLUSION

The pathway for the formation of CdSe QBs elucidated in this study is a potentially general explanation for the origin of the colloidal plate- and belt-like nanocrystals that have been recently discovered. We find that QB formation is mediated by double-lamellar template structures formed in the long-chain primary amine solvent, and that the dimensions of the template structures are responsible for the widths, thicknesses, and lengths of the QBs. The lamellar-template growth pathway appears to be responsible for the excellent optical properties of the QBs. We also find that $(CdSe)_n$ nanoclusters are stabilized within the amine templates, such that the nanocluster−QB conversion is reversible. Future work will be aimed at controlling the template structures to achieve purposeful control of plate or belt morphologies and their dimensions.

ASSOCIATED CONTENT

Supporting Information. Additional XRD patterns, and extinction and photoluminescence spectra. This material is available free of charge via the Internet at http://pubs.acs.org.

AUTHOR INFORMATION

Corresponding Author
*buhro@wustl.edu

ACKNOWLEDGMENT

This work was supported by the NSF under grant CHE-1012898.

REFERENCES

(1) Joo, J.; Son, J. S.; Kwon, S. G.; Yu, J. H.; Hyeon, T. *J. Am. Chem. Soc.* **2006**, *128*, 5632–5633.
(2) Son, J. S.; et al. *Angew. Chem., Int. Ed.* **2009**, *48*, 6861–6864.
(3) Ithurria, S.; Dubertret, B. *J. Am. Chem. Soc.* **2008**, *130*, 16504–16505.
(4) Ithurria, S.; Bousquet, G.; Dubertret, B. *J. Am. Chem. Soc.* **2011**, *133*, 3070–3077.
(5) Liu, Y.-H.; Wayman, V. L.; Gibbons, P. C.; Loomis, R. A.; Buhro, W. E. *Nano Lett.* **2009**, *10*, 352–357.
(6) Murray, C. B.; Norris, D. J.; Bawendi, M. G. *J. Am. Chem. Soc.* **1993**, *115*, 8706–8715.
(7) Peng, Z. A.; Peng, X. *J. Am. Chem. Soc.* **2002**, *124*, 3343–3353.
(8) Peng, Z. A.; Peng, X. *J. Am. Chem. Soc.* **2001**, *123*, 1389–1395.
(9) Manna, L.; Scher, E. C.; Alivisatos, A. P. *J. Am. Chem. Soc.* **2000**, *122*, 12700–12706.
(10) Kan, S.; Mokari, T.; Rothenberg, E.; Banin, U. *Nat. Mater.* **2003**, *2*, 155–158.
(11) Trentler, T. J.; Hickman, K. M.; Goel, S. C.; Viano, A. M.; Gibbons, P. C.; Buhro, W. E. *Science* **1995**, *270*, 1791–1794.
(12) Hollingsworth, J. A.; Poojary, D. M.; Clearfield, A.; Buhro, W. E. *J. Am. Chem. Soc.* **2000**, *122*, 3562–3563.
(13) Dong, A.; Tang, R.; Buhro, W. E. *J. Am. Chem. Soc.* **2007**, *129*, 12254–12262.
(14) Tang, Z.; Kotov, N. A.; Giersig, M. *Science* **2002**, *297*, 237–240.
(15) Tang, Z.; Zhang, Z.; Wang, Y.; Glotzer, S. C.; Kotov, N. A. *Science* **2006**, *314*, 274–278.
(16) Srivastava, S.; Santos, A.; Critchley, K.; Kim, K.-S.; Podsiadlo, P.; Sun, K.; Lee, J.; Xu, C.; Lilly, G. D.; Glotzer, S. C.; Kotov, N. A. *Science* **2010**, *327*, 1355–1359.
(17) Schliehe, C.; Juarez, B. H.; Pelletier, M.; Jander, S.; Greshnykh, D.; Nagel, M.; Meyer, A.; Foerster, S.; Kornowski, A.; Klinke, C.; Weller, H. *Science* **2010**, *329*, 550–553.
(18) Yu, J. H.; et al. *Nat. Mater.* **2010**, *9*, 47–53.
(19) Pradhan, N.; Xu, H.; Peng, X. *Nano Lett.* **2006**, *6*, 720–724.
(20) Huang, X.; Roushan, M.; Emge, T. J.; Bi, W.; Thiagarajan, S.; Cheng, J.-H.; Yang, R.; Li, J. *Angew. Chem., Int. Ed.* **2009**, *48*, 7871–7874.
(21) Rempel, J. Y.; Trout, B. L.; Bawendi, M. G.; Jensen, K. F. *J. Phys. Chem. B* **2006**, *110*, 18007–18016.
(22) Milliron, D. J.; Hughes, S. M.; Cui, Y.; Manna, L.; Li, J.; Wang, L.-W.; Paul Alivisatos, A. *Nature* **2004**, *430*, 190–195.
(23) Riehle, F. S.; Bienert, R.; Thomann, R.; Urban, G. A.; Krüger, M. *Nano Lett.* **2009**, *9*, 514–518.
(24) Yu, T.; Joo, J.; Park, Y. I.; Hyeon, T. *J. Am. Chem. Soc.* **2006**, *128*, 1786–1787.
(25) Park, K. H.; Jang, K.; Son, S. U. *Angew. Chem., Int. Ed.* **2006**, *45*, 4608–4612.
(26) Puntes, V. F.; Zanchet, D.; Erdonmez, C. K.; Alivisatos, A. P. *J. Am. Chem. Soc.* **2002**, *124*, 12874–12880.
(27) Park, K. H.; Choi, J.; Kim, H. J.; Oh, D.-H.; Ahn, J. R.; Son, S. U. *Small* **2008**, *4*, 945–950.

(28) Sasaki, T.; Ebina, Y.; Kitami, Y.; Watanabe, M.; Oikawa, T. *J. Phys. Chem. B* **2001**, *105*, 6116–6121.
(29) Manna, L.; Wang; Cingolani, R.; Alivisatos, A. P. *J. Phys. Chem. B* **2005**, *109*, 6183–6192.
(30) Sun, M.; Yang, X. *J. Phys. Chem. C* **2009**, *113*, 8701–8709.
(31) Kuçur, E.; Ziegler, J.; Nann, T. *Small* **2008**, *4*, 883–887.
(32) Dukes, A. D.; McBride, J. R.; Rosenthal, S. J. *Chem. Mater.* **2010**, *22*, 6402–6408.
(33) Del Ben, M.; Havenith, R. W. A.; Broer, R.; Stener, M. *J. Phys. Chem. C* **2011**, *115*, 16782–16796.